Precision Engineering 81 (2023) 145–157

Contents lists available at ScienceDirect

Precision Engineering

journal homepage: www.elsevier.com/locate/precision

Calibration of machine platform nonlinearity in Instrumented Indentation Test in the macro range

Jasurkhuja Kholkhujaev [a,b], Giacomo Maculotti [b,*], Gianfranco Genta [b], Maurizio Galetto [b]

[a] Turin Polytechnic University in Tashkent, Kichik Halka Yuli, 17, Tashkent, Uzbekistan
[b] Department of Management and Production Engineering, Politecnico di Torino, Corso Duca Degli Abruzzi 24, 10129, Turin, Italy

ARTICLE INFO

Handling Editor: R. Leach

Keywords:
Calibration
Measurement uncertainty
Instrumented Indentation Test
Frame compliance
Spring stiffness
Nonlinear spring

ABSTRACT

Instrumented Indentation Test (IIT) is a non-conventional mechanical characterization technique to evaluate hardness, Young modulus, creep and relaxation of materials. In the macro range, it represents a cheaper and faster alternative to conventional tensile-based tests. IIT is a metrological scale; thus, to establish traceability, calibration is essential. Frame compliance calibration is critical because it is a major contribution to the measurement uncertainty. This work discusses the limits of the current state-of-the-art and proposes a novel methodology for frame compliance calibration. The introduced approach demonstrates the source of common systematic errors in the mechanical characterization reported in the literature, i.e. edge effect, while first highlighting a relevant frame compliance nonlinearity. The proposed procedure is cost-effective and relies upon constitutive spring modelling of IIT and calibration of reference block by nanoindentation. Results show that the novel approach corrects systematic trends in the characterization and yields a relative measurement uncertainty of 5%.

1. Introduction

Instrumented Indentation Test (IIT) is a non-conventional hardness test, standardized by ISO 14577 [1]. It consists in applying by an indenter a loading-holding-unloading force-controlled cycle to indent a material that has to be characterized. Differently from conventional hardness tests, the indenter penetration in the material is continuously measured throughout the cycle. The measurement results in an indentation curve (IC), relating the applied force (F) to the resulting indenter penetration depth in the material (h), as shown in Fig. 1.

IIT can be applied at different scales: nano ($h < 0.2$ μm), micro ($F < 2$ N, $h > 0.2$ μm) and macro ($2\ \text{N} \leq F \leq 30$ kN) [1]. Thus, Instrumented Indentation Test represents a convenient mechanical characterization technique that allows a thorough characterization, e.g. in terms of the estimate of Young modulus, i.e. the indentation modulus E_{IT}, and indentation hardness, H_{IT}, on a multi-scale. . At the nanoscale, the instrumented indentation test allows characterizing grains of material, differentiating between different phases [3,4] and average size [5], and nano-structures [6]. Conversely, the macro-scale is a convenient alternative to a destructive test, e.g. tensile test, which does not require an ad-hoc shaped specimen but can be performed on the final component [7]. Therefore, it may provide a reduction of scraps and a more representative characterization of the real component material. At the macro scale, it proved effective in characterizing average material properties while still distinguishing the presence of surface treatments and residual stresses [7–10]. Furthermore, IIT is directly traceable, thanks to the calibration of the force and displacement scale sensors, which provide end users with confidence in the obtained results [11]. Consequently, within the European Green Deal and the current sustainability framework, it may represent a quality control inspection method suitable for obtaining robust results while reducing waste [12]. IIT is a viable solution to establish a correlation to physical quantities of conventional and non-metrological mechanical tests, e.g. Rockwell [11,13,14]. Therefore, ensuring traceability via calibration to provide end users with high metrological performances in terms of accuracy and precision is essential. This work focuses on the calibration of Instrumented Indentation Test in the macro range.

1.1. Characterization method

The characterization method requires the analysis of the IC curve. In particular, the indenter displacement measured data, h_m, require first

* Corresponding author.
E-mail address: giacomo.maculotti@polito.it (G. Maculotti).

https://doi.org/10.1016/j.precisioneng.2023.02.005
Received 27 September 2022; Received in revised form 28 December 2022; Accepted 10 February 2023
Available online 15 February 2023

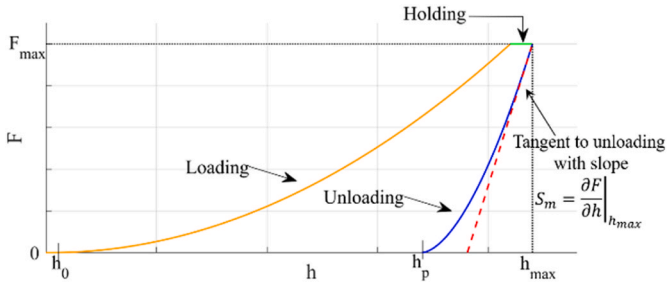

Fig. 1. Indentation Curve (IC) with loading-holding-unloading phase and main characterisation parameters [2].

the correction of systematic error contribution, to obtain the corrected displacement, h_c:

$$h_c = h_m - h_0 - C_f F - \varepsilon F/S \tag{1}$$

where C_f is the machine platform compliance, i.e. the frame compliance, the ε is a constant depending on the indenter geometry, and S is the sample contact stiffness. Accordingly, the corrected errors include: the zero error (h_0), i.e. the first contact point between the indenter and the sample, the elastic deformation of the machine, i.e. $C_f F$, and the elastic deformation of the sample, i.e. $\varepsilon F/S$. The contact stiffness is evaluated by modelling the system as a series of springs, see Fig. 2, modelling the compliance of the machine, C_f, and the stiffness of the sample, S. In the most typical cases, the used indenter has a Vickers geometry, i.e. an $\varepsilon = 0.75$.

The mechanical characterization is obtained as:

$$H_{IT} = \frac{F}{A_p(h_{c,max})} \tag{2}$$

$$E_{IT} = \frac{1-\nu_s^2}{\frac{2\sqrt{A_p(h_{c,max})}}{S\sqrt{\pi}} - \frac{1-\nu_i^2}{E_i}} \tag{3.1}$$

$$\frac{2\sqrt{A_p(h_{c,max})}}{S\sqrt{\pi}} = \frac{1}{E_r} \tag{3.2}$$

where ν_s is the sample Poisson modulus; ν_i and E_i are the Poisson and Young modulus of the indenter, respectively; A_p is the projected contact area, and often, the ratio $\frac{2\sqrt{A_p(h_{c,max})}}{S\sqrt{\pi}} = \frac{1}{E_r}$ is referred to through the reduced modulus, E_r.

Therefore the characterization requires preliminarily evaluating the projected contact area, A_p, at the maximum penetration depth, $h_{c,max}$, and the contact stiffness S.

The projected contact area is typically a function of the penetration depth through a set of parameters ϑ that require calibration, i.e. $A_p(h_{c,max};\vartheta)$, and whose functional form is dependent on the indenter geometry. In the simpler case of macro instrumented indentation performed with a Vickers indenter, the area shape function is:

$$A_p(h_c) = 24.56 h_c^{\,2} \tag{4}$$

which does not include corrective terms for the deviation from ideal indenter geometry, for these are negligible at the characterization scale [15].

The contact stiffness is obtained by the spring model, see Fig. 2, correcting the measured total stiffness, S_m, by the frame compliance, C_f:

$$\frac{1}{S_m} = C_{tot} = C_f + \frac{1}{S} \tag{5.1}$$

$$S_m = \frac{\partial F}{\partial h}\Big|_{h=h_{m,max}} \tag{5.2}$$

where the total measured stiffness can be calculated as the derivative of the IC at the onset of the unloading, and several analytical and numerical methods are available for this operation [16–19]. In this work, the standard power law method is used [1,17,19].

1.2. State-of-the-art calibration methods

The standard requires calibrating the measurement scales, i.e. the force and displacement transducers, the penetrator tip geometry and the frame compliance [20]. In particular, the latter has been demonstrated to significantly affect the characterization results both in terms of bias and precision, and its effect dominates in the macro range other influence factors to measurement uncertainty, e.g. the adoption of the ideal indenter area shape function [18,21]. The literature and the standard propose several calibration methods for the frame compliance [2,20,22]. However, several limitations are present [23] and, despite calibration being performed, characterization results are often biased and affected by systematic trends [13,14]. The most relevant approaches for calibration are those reported in the ISO 14577–2:2015 [20] and in the review by Ullner et al. [22] and are described in the following. Literature and standard [20,22,24] require performing a set of indentations of a very hard material, and analyzing the results according to different approaches to estimate the frame compliance. The choice of the very hard material aims to minimize the sample elasticity and elastic deformation effect on the measurements. The good practice originated for the application in the nano-range, suggesting the use of tungsten [2], alumina [20], and sapphire [24], and then generalized to hard grades of

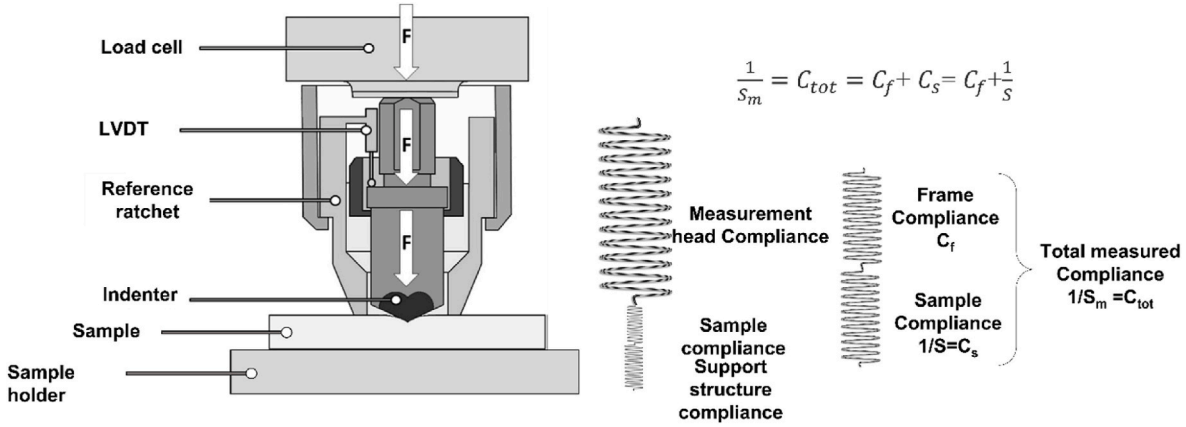

Fig. 2. Spring model of the indentation platform (modified from Ref. [18]). On the left a functional scheme of the main components of the indentation system and on the right the spring model representing the frame and sample compliance.

steels for the macro range [13,14,18].

1.2.1. ISO 14577-2 methods

The standard ISO 14577-2 in Annex D reports several frame compliance calibration methods. However, despite the standard aims at all the application ranges of IIT, all the calibration methods were conceived for applications in the nano range, and the standard's examples and good practice guides are limited to the nano range. By extrapolation, only the second method from ISO 14577–2:2015 Annex D is applicable in the macro range [13,14,23]. The approach requires performing a set of indentations at different loads and analysing the results by an iterative procedure, shown in Fig. 3, that is terminated upon convergence. The underlying hypothesis of the method assumes a constant frame compliance. The approach also requires the use of a calibrated reference block in terms of Young modulus, E, or indentation modulus, E_{IT}. The literature addressed the flaws of this approach in the high sensitivity to the experimental set-up, i.e. calibrated force range, number of force levels and replication [25,26]. Moreover, when applied to the macro range, the approach results in bias, sometimes ascribed to plasticity effects of the indentation, i.e. edge effects [13,14]. However, edge effects, typically presenting as pile-up or sink-in, are negligible in the macro range and primarily affect micro and nano range applications [27–30].

1.2.2. C_{tot} vs $F^{0.5}$ linear regression approach

Although not included in the standard, the method is reviewed in Ullner et al. [24] and applied in relevant state-of-the-art literature [18]. It operates under the assumption of a constant H_{IT}/E_r^2 ratio, and hypotheses that the frame compliance is constant through the whole operating range of the indentation platform. The procedure estimates by linear regression the C_f as the intercept of the model reported in Eq. (6), which is obtained by rearranging Eqs. (2), (3) and (5):

$$C_{tot} = C_f + \frac{\sqrt{\pi H_{IT}}}{2E_r}\frac{1}{\sqrt{F}} \tag{6}$$

Literature shows that this approach may induce a bias and systematic trends in the results [13,18]. Moreover, it requires a calibrated value of the reduced modulus E_r and indentation hardness H_{IT}, which is typically not reported. Furthermore, it is worth stressing that the constant H_{IT}/E_r^2 assumption, at the macro range, is equivalent to assume that both E_r and H_{IT} are constant. In fact, the reduced modulus definition can also be rewritten as:

$$E_r = \left(\frac{1-\nu_s^2}{E} + \frac{1-\nu_i^2}{E_i}\right)^{-1} \tag{7}$$

which is constant by the definition of Young modulus, hence leading to a requirement of a constant H_{IT}. A constant hardness evaluation is particularly challenging because it is highly dependent on evaluation scale. In fact, it can be affected by indentation size effect (ISE) [5] at the lower end and by edge-effect at the higher end of nano and micro instrumented indentation test [30].

1.2.3. Other methods

Literature also presents additional methods. An alternative solution relies on calibrated samples in terms of Martens hardness [22]. However, this approach does not allow establishing traceability for the Young's modulus. Therefore, the accuracy of E_{IT} cannot be evaluated. Another recently introduced alternative exploits indentations replicated in the same position at the same load. However, although interesting, it presents some modelling criticalities that lead to an evaluation of the frame compliance dependent on the calibration material [13,14], which is inconsistent with the definition of frame compliance. Therefore, these methods will not be considered in this work as a benchmark.

1.3. Scope of the work

The literature review shows that the current calibration procedure for the frame compliance presents some limitations and primarily relies on a constant frame compliance assumption. However, no spring can be modelled as ideally linear on a wide range of forces, as it is the force operating range of common macro indentation platforms [31,32]. Moreover, in the case of indentation platforms, mating with gaps, kinematics, and complex assembly make such assumption extremely critical [24]. This work proposes a calibration methodology to cater for the machine compliance nonlinearity based on a set of indentations performed on a reference material calibrated by a novel multi-scale characterization approach via instrumented indentation test.

The rest of the paper is structured as follows. Section 2 first describes the experimental set-up and applies state-of-the-art calibration methods to show the main criticalities and allow more insight. Then, it describes the novel calibration method that caters for frame compliance nonlinearity, also focusing on the approaches to guarantee traceability and evaluating the measurement uncertainty. Section 3 describes the results of the calibration method when applied to several materials for validation purposes and compares the results with other state-of-the-art calibration approaches reported in the literature. Finally, Section 4 draws the conclusions.

2. Materials and methods

2.1. Experimental set-up

This work focuses on the calibration of instrumented indentation platform for the macro range ISRHU09 [18] by AXIOTEK S.a.s. The

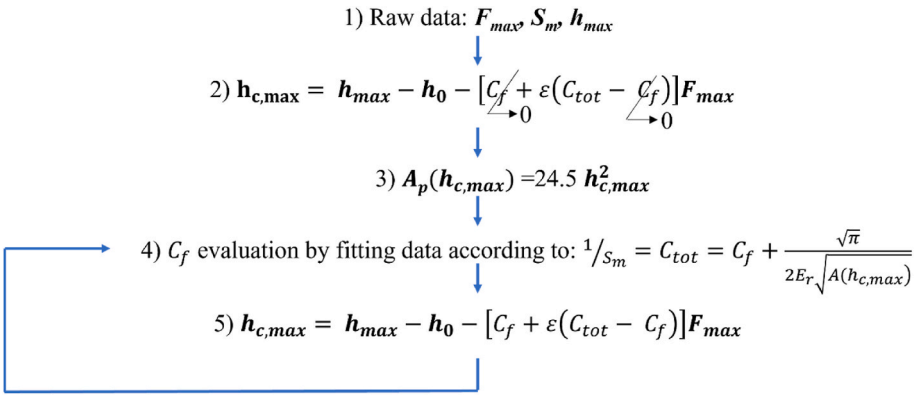

Fig. 3. Workflow of the standard calibration of the frame compliance as per method 2 of Annex D of ISO 14577–2:2015. Bold quantities are vectors of collected data of replicated measurements of several load forces.

indentation platform is hosted in the metrological room of the Mind4Lab (Manufacturing for Industry 4.0 Laboratory) at the Department of Management and Production Engineering of Politecnico di Torino and is shown in Fig. 4. The platform features the range, resolution and metrological characteristics of force and displacement reported in Table 1. The force scale is realized by a force transducer and was calibrated with reference to ISO 14577–2:2015 [20] and ISO 376:2011 [33]. The displacement scale features a LVDT sensor, calibrated as per ISO 14577–2:2015 [20]. Calibrations were performed with the support of Italian National Metrological Institute, i.e. the Istituto Italiano di Ricerca Metrologica (INRiM), and the indentation platform manufacturers.

Indentations to calibrate the frame compliance of the macro-instrumented indentation platform have been performed on calibrated conventional hardness reference blocks out of Aluminium, Brass, and two grades of stainless steel, as reported in Table 2, with a Vickers indenter with a calibrated half dihedral angle of (68.03 ± 0.05)°.

2.2. Calibration of reference blocks

In this work, the calibration of the reference block for macro-IIT is performed in terms of indentation modulus and indentation hardness by nano- and micro-IIT. This calibration is necessary to implement and hence compare the frame compliance calibration methods described in Section 1.2.

The calibration method consists of performing a set of indentations from the nano-to the micro-range by a calibrated instrumented indentation platform and evaluating as a result the E_{IT} and the H_{IT} in absence of systematic effect.

A state-of-the-art calibrated instrumented indentation platform STeP6 by Anton Paar hosted in the facilities of the Mind4Lab metrological room of the Politecnico di Torino was used. The indentation platform features two measurement heads, i.e. an NHT^3 with an operating force range of (0.1–500) mN and an MCT^3 with an operating force range of (500 mN–30 N), for the nano- and the micro-instrumented indentation test, respectively. The NHT^3 sensor features a force-displacement piezoelectric sensor, whilst the MCT^3 a load transducer and an LVDT. Direct calibration of both measurement heads' force and displacement scales was performed as per ISO 14577–2:2015 by the manufacturer. Frame compliance calibration was performed in accordance with standard practice on fused silica and BK7 glass samples calibrated by frequency resonance by National Physical Laboratory (NPL) in terms of plain strain and elastic modulus. The resulting indentation hardness.

Fig. 4. The calibrated macro instrumented indentation platform ISRHU09 by AXIOTEK.

The calibration of the reference blocks has been obtained by evaluating the H_{IT} as a function of the applied load. The trend allows identifying three load ranges: (i) at very low characterization scales, a range affected by ISE, which induces a systematic increase of the mechanical properties as the characterization force decreases [35,36]; (ii) at large characterization scale, relative to the nano- and micro-range, a load range affected by edge effects, i.e. pile-up or sink-in, which generates a systematic increase or decrease of the material properties as the characterization load increases; (iii) an intermediate range, nominally unaffected by those errors [5,27,30]. The reference indentation modulus E_{IT}, indentation hardness $H_{IT,}$ and reduced modulus E_r can be evaluated as the average in the intermediate load range. Expanded uncertainty of the characterization can be determined by propagating the contribution of the influence factors on mechanical characterization result [19,21]. The hardness trend as a function of the load analysis is critical and it is essential to remove edge effect-affected, i.e. biased, indentations. The identification of the unbiased region, i.e. the intermediate range, can be performed basing on the H_{IT} trend, and here is complemented with surface topography measurement of the indentations to provide a qualitative assessment of the impact of the edge effect. Indentations in the unbiased force scale and in the edge-effect affected force scale have been measured. The measurement of the surface topography is performed by a state-of-the-art surface topography measuring instrument, namely a coherence scanning interferometry [37] NewView 9000 by Zygo hosted in the metrological room of the Mind4Lab of Politecnico di Torino. Surface topography measurements have been performed with a 20 × Mirau objective, with a numeric aperture of 0.4, a squared pixel size of 0.43 μm; smaller indentations, i.e. those on harder materials, were performed with a 50 × Mirau objective, with a numeric aperture of 0.55, a squared pixel size of 0.17 μm. In any case, one field-of-view of 1000 × 1000 pixel was sufficient to measure indentations at any force scale. A quantitative estimate of the pile-up can be provided by the ratio $h_{pu}/h_{c,max}$, where the numerator is the height of the pile-up, estimated from the surface topography measurement, and the denominator is the maximum corrected depth, at which mechanical characterizations are performed. This ratio indicates a relevant pile-up when exceeding the 20%. No significant pile-up can be assumed when smaller than 10%. In between those value the distribution of the pile-up and actual area might impact on the induced bias [5,27,29,30].

The four reference blocks reported in Table 2 are accordingly characterized by performing 10 replicated indentations in a characterization range of (50 mN–30 N) with conventional indentation cycles with a loading time of 30 s, a holding of 30 s, and unloading of 30 s [38] with a modified Berkovich indenter.

The proposed methodology for calibrating reference block is alternative to common alternatives and features several advantages. The calibration is typically performed by the frequency resonance method, which allows characterizing the Young modulus with great precision and accuracy by a non-destructive test. However, this approach has twofold limitations. First, it is limited to a few well-defined geometries of the reference blocks, which should also be sufficiently small [34], which makes the approach suitable for nanoindentation reference blocks calibration, but may be impractical for macro-scale references. In fact, blocks for macro Instrumented Indentation Test require a larger size, and hence weight, to allow convenient reusability. Second, it does not allow calibrating the indentation hardness. Moreover, no approaches to calibrate the indentation hardness are reported. This generates criticalities to estimate and verify the hypothesis of state-of-the-art approaches. Furthermore, no calibration service neither from accreditation

Table 1
Force and Displacement metrological characteristics of the considered indentation platform. Displacement accuracy could not be evaluated due to a relatively poor resolution of the LVDT.

Scale	Range	Resolution	Accuracy	Reproducibility	Inversion error
Force	(100–2500) N	85 mN	0.30%	0.40%	0.2%
Displacement	±160 μm	8 nm	–	60 nm	−0.3%

Table 2
Reference blocks materials and calibrated conventional hardness values reported as average and expanded uncertainty (coverage factor k = 2).

Material	Acronym in this paper	Calibrated conventional hardness
Aluminium	Al	(36.6 ± 1.8) HRA
Brass	BR	(62.4 ± 0.3) HRB
Stainless Steel (softer)	SSs	(63.9 ± 3.2) HRA
Stainless Steel (harder)	SSh	(64.3 ± 0.1) HRC

laboratories nor from National Metrological Institutes offers such calibration for metallic materials, but only for amorphous materials that are suitable only for nanoindentation.

2.3. Literature frame compliance calibration methods

State-of-the-art approaches reported in Section 1.2 are applied to the considered platform to highlight and demonstrate the main criticalities and drawbacks on a practical case. For both approaches (standard method, M-ISO, and state-of-the-art literature method, M-SOA), a set of 10 replications at 12 force levels within the operating range of the ISRHU09 machine, i.e. [100, 150, 200, 250, 300, 400, 500, 600, 700, 800, 900, 1000] N, were performed on the hardest material available, i.e. the hard stainless steel (SSh), as per good practices, considering the calibrated material properties as described in Section 2.2. Conventional indentation cycles with a loading time of 60 s, a holding of 30 s, and unloading of 60 s were performed [38].

2.4. A novel calibration method for frame compliance nonlinearity

The current calibration framework exploits the spring model of the indentation system and works under the non-trivial assumption of a constant frame compliance. However, macro indenters operating on a range of hundreds of kilograms, presenting several mechanical matings with gaps and kinematics, make such assumption quite hard to be verified.

The proposed method modifies the approach presented in Section 1.2.2. Considering the spring model of Eq. (5), the frame compliance C_f can be rewritten as:

$$C_f = C_{tot} - \frac{1}{S} = \frac{1}{S_m} - \frac{1}{S} = \frac{1}{S_m} - \frac{\sqrt{\pi H_{IT}}}{2E_r}\frac{1}{\sqrt{F}} \tag{8}$$

This expression conceptually allows determining the approximation degree introduced by the constant compliance assumption.

Operationally, the procedure requires performing a set of replicated indentations on a calibrated reference block in terms of indentation modulus and indentation hardness at several load levels within the operating range of the indentation platform to be calibrated. The C_f is evaluated by performing a linear regression, having as regressor the force, which is also the measured quantity with the smallest uncertainty in the measured system [18], and henceforth allows applying an ordinary least-square regression [2]. The empirical estimates of the C_f rely on the calibration of the mechanical quantities and the empirical evaluation of the contact stiffness. From a practical perspective, the proposed approach is more general, for it includes the possibility of load-independent frame compliance.

2.4.1. Uncertainty evaluation

The standard uncertainty of the calibrated frame compliance is obtained by propagating contributions through the law of uncertainty propagation, in accordance with the Guide to the expression of uncertainty in measurements (GUM) [39]. Let the regression model for Eq. (8) be rewritten, highlighting all the contributions to measurement uncertainty, i.e. the regressor and the estimated parameters:

$$C_f = f(\boldsymbol{x}) = f\left(\frac{1}{\sqrt{F}}, a, b, \varepsilon\right) = a + b\frac{1}{\sqrt{F}} + \varepsilon \tag{9.1}$$

$$a = \widehat{\frac{1}{S_m}}, A \sim N\left(\overline{\frac{1}{S_m}}, SE_a^2\right) \tag{9.2}$$

$$b = -\widehat{\frac{\sqrt{\pi H_{IT}}}{2E_r}}, B \sim N\left(\overline{-\frac{\sqrt{\pi H_{IT}}}{2E_r}}, SE_b^2\right) \tag{9.3}$$

$$\varepsilon = C_f - \widehat{C_f}, E \sim N(0, MSE_\varepsilon) \tag{9.4}$$

where SE_a is the standard error of the estimated parameter a, and its square is a correct and unbiased estimator of the parameter variance, i.e. $SE_a^2 = \widehat{\mathbb{V}ar}[a]$, ε are the residuals. Then, the uncertainty propagation can be written as:

$$u(y)^2 = \boldsymbol{c}^T \boldsymbol{V} \boldsymbol{c} \tag{10.1}$$

$$c_{i,j} = \left.\frac{\partial f}{\partial \boldsymbol{x}}\right|_{x=x_0} \tag{10.2}$$

$$\boldsymbol{V} = \begin{bmatrix} SE_a^2 & cov(a,b) & 0 & 0 \\ cov(a,b) & SE_b^2 + u_{b,trac}^2 & 0 & 0 \\ 0 & 0 & u(F)^2 & 0 \\ 0 & 0 & 0 & MSE_\varepsilon \end{bmatrix} \tag{10.3}$$

where $\boldsymbol{c}$ is the sensitivity coefficient array, and $\boldsymbol{V}$ is the variance-covariance matrix that includes the variance-covariance of the regression-estimated parameters, the variance $u(F)^2$ of the independent variable, the variance of the residuals MSE_ε, and $u_{b,trac}^2$ propagates the traceability of the calibrated reference indentation hardness and reduced modulus; the traceability is computed by combining the law of variance propagation for the analytic expression of the parameter b on the uncertainty of the calibrated parameters as per the methodology detailed in Section 2.2.

2.4.2. Reference material choice

Some literature is currently ascribing systematic errors in macro instrumented indentation test characterization to the plasticity of the material, rather than nonlinear frame compliance, despite the relative amount of error introduced by pile-up and sink-in is orders of magnitude smaller than the penetration depth. To disproof such hypotheses and further prove the validity of the proposed approach, qualitative investigations of indentations are performed on the material. These are carried out by measuring the surface topography of the indentations with the coherence scanning interferometry Zygo NewView 9000 with the 20 × objective and evaluating the ratio $h_{pu}/h_{c,max}$.

According to good practice, calibration will be performed with the

hardest material available. Additionally, other alternatives will be considered, and results compared. The scope of this analysis is to show that if the reference block is adequately calibrated and at the macro characterization scale it does not present any edge effect, no systematic trend is induced in the characterization results, and the choice of the calibration material is ultimately irrelevant, in the macro range.

2.5. Validation approach

The validation of the calibration methods presented in Section 1.2 and Section 2.4 is performed by comparing the characterization results obtained, including the calibrated frame compliance correction, with the calibrated values. The characterization considers both the E_{IT} and the H_{IT} at different loads. The same experimental set-up exploited to gather the calibration indentations set will also be used for validation (see Section 2.1). Validation tackles all the materials reported in Table 2. The comparison is based on a hypothesis test on the means, with a null hypothesis H_0: $m_i = m_{Ref}$, where m_i is the characterization mean obtained with the i-th calibration method, and m_{Ref} the related calibrated value. The null hypothesis will be rejected with a risk of error of 5% if

$$\frac{|m_i - m_{Ref}|}{\sqrt{u_i^2 + u_{Ref}^2}} > t_{\nu,97.5}^{-1} \tag{11}$$

where the left-hand side distributes as a t-Student with ν degrees of freedom, and the right-hand side is the quantile of the t-Student with ν degrees of freedom whose cumulated probability is 97.5%. The denominator combines the standard uncertainty of the characterized and calibrated mechanical properties. A graphical way to perform such a test is to verify if error bars plot with error bars as wide as the expanded uncertainty overlap with the uncertainty-based confidence interval of the calibrated reference values.

Standard uncertainties are evaluated by propagating through Eq. (2) and Eq. (3) all relevant contributions, including the measurement reproducibility, from the 10 replicated indentations, and specifically the standard uncertainty of the calibrated frame compliance [18,21,39]. Uncertainty propagation is performed according to the GUM [39]. Standard uncertainty of the calibrated frame compliance is evaluated according to the GUM [39] as the standard error of estimated regression parameters, associating a normal distribution, for all the literature methods are linear regressions. As far as the proposed approach is concerned, the uncertainty evaluation of the frame compliance has been addressed in Section 2.4.1.

3. Results and discussion

3.1. Calibration of reference blocks

Fig. 5 shows the results of the characterized conventional hardness blocks in terms of indentation hardness H_{IT}. The results, consistent with the literature, highlight the three load ranges in terms of characterization force scale, i.e. indentation size effect-affected force scales, accurate characterization force scale and edge effect-affected force scale. In the load range where H_{IT} may be assumed constant, a calibrated reference value of mechanical characterization by instrumented indentation test can be computed as average and expanded uncertainty of the collected data. Results are shown in Table 3 as average and expanded uncertainty at a 95% confidence level; in accordance with the literature [21], the uncertainty is dominated by the reproducibility contribution.

Complementary surface topography measurements were performed to show the presence of edge effect, consistently with the indentation

Table 3
Calibrated mechanical characteristics of the considered materials by nano- and micro-instrumented indentation. Intervals represent expanded uncertainty at a 95% confidence level.

Material	E_{IT}/GPa	E_r/GPa	H_{IT}/GPa
Al	72.74 ± 2.19	76.10 ± 2.48	1.10 ± 0.02
BR	93.99 ± 5.40	94.36 ± 1.97	1.27 ± 0.03
SSs	190.58 ± 5.29	175.39 ± 3.49	3.45 ± 0.16
SSh	198.607 ± 4.48	181.31 ± 1.95	9.87 ± 0.33

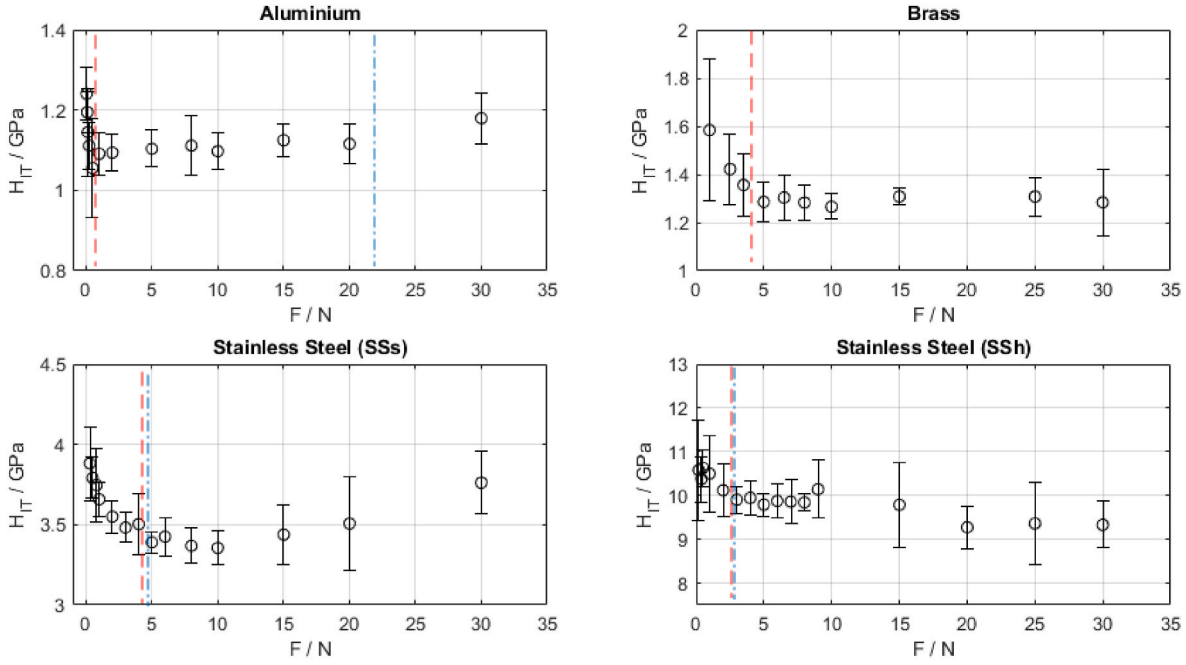

Fig. 5. Reference material characterization with a calibrated nano- and micro-instrumented indentation test. Red dashed lines highlight Indentation Size Effect at smaller loads, blue dot-dashed lines identify edge effect at higher loads. Depending on the plasticity of the material, edge effects are onset at different loads. Edge effect cannot be appreciated in the Brass, whilst a region unaffected by edge effect cannot be highlighted in SS, as shown by the red and blue line positioning. ISE can always be appreciated. (For interpretation of the references to colour in this figure legend, the reader is referred to the Web version of this article.)

hardness presenting an increasing trend. In fact, if the material piles up at the indentation edge, the actual contact area is greater than the one computed from characterization equations, see Eq. (1) and Eq. (4). The contact area underestimation induces an increase in the evaluated hardness, see Eq. (2) [29,30]. The pile-up behaviour depends on the yield strength-to-Young modulus ratio and the work hardening coefficient of the material. Brass shows no edge effect with a $h_{pu}/h_{c,max} = 9.5\%$, as shown in Fig. 6. Aluminium presents a $h_{pu}/h_{c,max} = 14.8\%$ in the constant load scale region, indicating a marginal pile-up as also confirmed by Fig. 7, which increases in severity up to a significant $h_{pu}/h_{c,max} = 21.1\%$ at higher loads. Both grades of stainless steels present a significant pile-up at high loads ($h_{pu}/h_{c,max} = 23\%$), as also shown in Figs. 8 and 9, respectively, for the softer and harder SS. The $h_{pu}/h_{c,max}$ allows insights in the severity of pile-up indicating a significative constant bias even in the force range, which yield a constant H_{IT}, presenting a value of the $h_{pu}/h_{c,max}$ ratio of 22%. Figures from 6 to 9 show a sample indentation at load scale unaffected by edge effect and at a load scale where pile up is relevant. The pile-up analysis by surface topography measurements suggests the possible presence of a bias in the characterization by nano and micro of stainless steels. In particular, the constant region (which is the middle one for the SSs and the second one for the SSh) can be interpreted as a region where the edge effect is present and constant rather than increasing with the load in severity. Therefore, it is reasonable to expect a systematic difference (a constant error, i.e. a bias, not a trend) between characterization results obtained at micro and macro scales.

3.2. Literature frame compliance calibration

3.2.1. ISO 14577-2 method (M-ISO)

The standardized approach (Section 1.2.1), M-ISO, reported as the second method of the Annex D of ISO 14577–2:2015 is applied, by performing indentations on the hardest stainless steel (SSh). In agreement with reference literature [13,14,18], a severe bias and trend can be seen in the characterization results in Fig. 10. Literature [13,14,18] tends to ascribe this to plasticity. The surface topography analysis shows that the amount of edge-effect, which, as discussed in Section 3.1 for the considered materials, entails pile-up, is negligible at the considered scales, i.e. in the macro range. This can be seen in Fig. 11, which reports the measured topographies of indentation performed at an arbitrarily set force of 400 N. Differently to what was reported at the micro-scale, neither qualitatively nor quantitatively, i.e. $h_{pu}/h_{c,max}$ resulted of 9.1%, 0.8%, 9.4% and 4.5% respectively for Al, Brass, SSs and SSh, no pile-up can be appreciated, which henceforth cannot be the cause of the bias in the results.

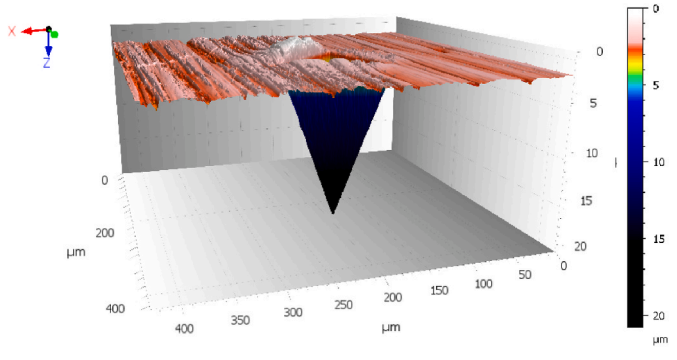

Fig. 6. Surface topography of instrumented indentation test on Brass sample at 10 N. A negligible pile-up can be observed, evenly distributed on the indentation edge. See supplementary material for further insights on the indentation topography.

3.2.2. C_{tot} vs $F^{0.5}$ linear regression approach (M-SOA)

Similarly, the same set of indentations, i.e. using as calibration material the SSh, were used to perform the calibration according to the state-of-the-art method (Section 1.2.2), M-SOA, based on the linear regression of the total compliance. Fig. 12 shows that in the C_{tot} vs $F^{-0.5}$ plane, which would allow a straight-line representation of the calibration model of Eq. (6) under the assumption of constant frame compliance, the C_{tot} trend is clearly nonlinear. This disproves the underlying hypothesis of the method, i.e. constant frame compliance. Provided the result shown in Fig. 12, no calibration of the frame compliance can be carried out without introducing a severe systematic error, and no further characterization is performed.

3.3. Nonlinear frame compliance calibration method

The proposed calibration approach that caters for nonlinear frame compliance is applied to the indentations set performed on Aluminium and Brass samples. This choice relies on the following consideration. The reference material has to be calibrated; in this work, we calibrated the materials according to the methodology described in Section 2.2, and related results in Section 3.1 showed that nano- and micro-instrumented indentation-based calibration may be biased for SS due to pile-up. Fig. 13 shows that the two estimated calibration trends of the C_f, i.e. considering the two calibrated materials, are compatible. In fact, the prediction intervals superimpose; hence, no systematic difference can be highlighted. Accordingly, the difference in the averages is not statistically significant. This proves that if the calibration of reference material is accurately performed, the choice of the material is irrelevant. Consequently, the proposed reference material calibration method in Section 2.2 provides consistent results when no significant pile-up at the micro-scale is present. This result is highly relevant, for by definition and ideally, the frame compliance is independent of the material used in its calibration.

In the following, results are shown considering the frame compliance calibration performed on Aluminium, for it is associated with a smaller uncertainty. The linear regression estimated a trend of the frame compliance according to Eq. (9), with parameters:

$$\hat{a} = 3.999 \bullet 10^{-6}\ \mathrm{mm/N} \tag{12.1}$$

$$\hat{b} = -2.119 \bullet 10^{-5}\ \mathrm{mm \bullet N^{-0.5}} \tag{12.2}$$

and a parameters variance-covariance matrix:

$$\begin{bmatrix} SE_a^2 & cov(a,b) \\ cov(a,b) & SE_b^2 \end{bmatrix} = \begin{bmatrix} 5.20 \bullet 10^{-15} & 8.8210^{-14} \\ 8.82 \bullet 10^{-14} & 1.02 \bullet 10^{-11} \end{bmatrix} \tag{12.3}$$

and a model, as per Eq. (9):

$$C_f = 3.999 \bullet 10^{-6}\ \mathrm{mm}\Big/\mathrm{N} + \frac{-2.119 \bullet 10^{-5}\ \mathrm{mm \bullet N^{-0.5}}}{\sqrt{F}} \tag{12.4}$$

The regression model presents an R^2 of 73%, and residual with a variance $MSE_e = 7.24 \bullet 10^{-14}$ mm/N, and normally distributed residuals, as qualitatively can be appreciated in Fig. 14(a) normal probability plot and confirmed by a quantitative χ^2 normality test, with a p-value of 0.333. The relatively low R^2 can be ascribed to the large dispersion of the empirical dataset, rather than to poor fitting performances. Uncertainty is propagated according to Section 2.4.1, and results in terms of prediction interval, with a confidence level of 95%, are shown in Fig. 14(b). For the uncertainty propagation, the traceability on the calibrated Aluminium mechanical properties resulted of $u_{b,trac}^2 = 8.4 \bullet 10^{-9}$ GPa, that corresponds to a relative expanded uncertainty for the traceability contribution of 1%.

The calibrated nonlinear frame compliance is then exploited to characterize the four considered materials, and results are shown from Figs. 15–18.

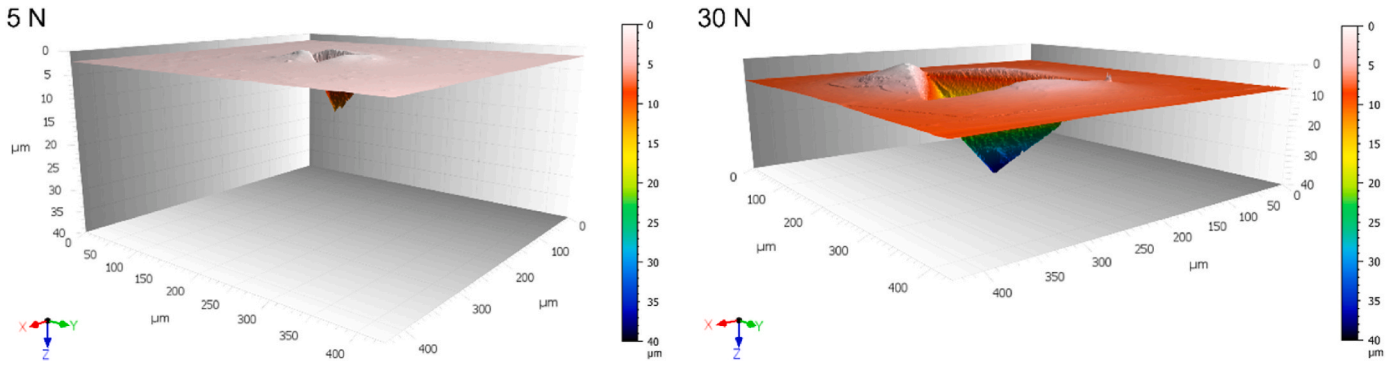

Fig. 7. Surface topography of instrumented indentation test on Aluminium sample at 5 N and 30 N. At higher loads pile-up is no more negligible, as also shown by the H_{IT} trend, showing an uneven distribution on the indentation edge. See supplementary material for further insights on the indentation topography.

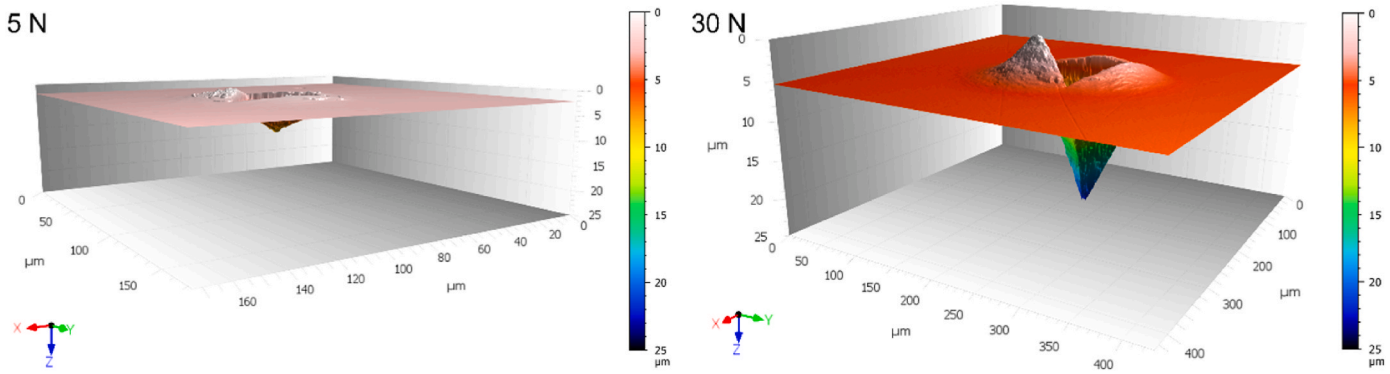

Fig. 8. Surface topography of instrumented indentation test on soft Stainless Steel (SSs) sample at 5 N and 30 N. At higher loads pile-up is no more negligible, as also shown by the H_{IT} trend, showing an uneven distribution on the indentation edge. See supplementary material for further insights on the indentation topography.

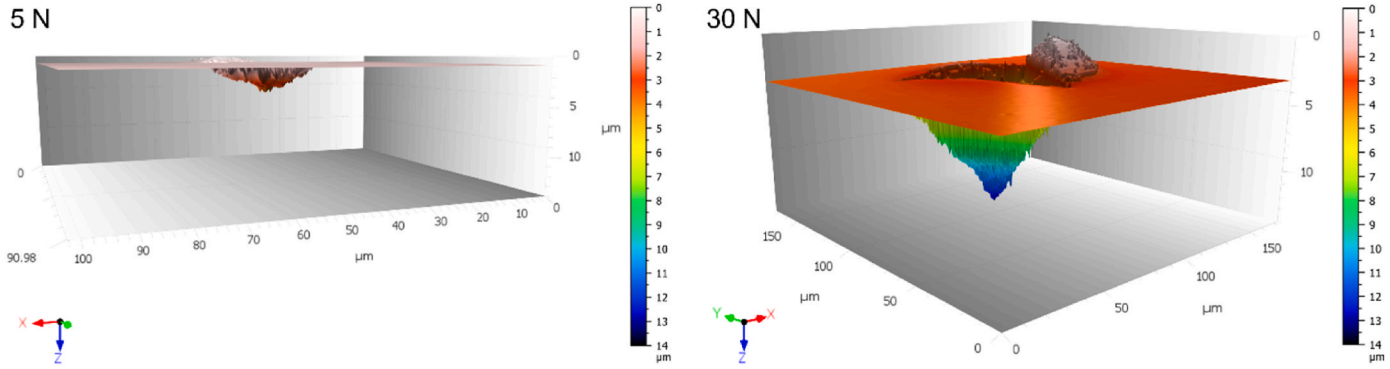

Fig. 9. Surface topography of instrumented indentation test on hard Stainless Steel (SSh) sample at 5 N and 30 N. At higher loads pile-up is no more negligible, as also shown by the H_{IT} trend, showing an uneven distribution on the indentation edge. See supplementary material for further insights on the indentation topography.

Aluminium characterization allows validating the calibration method, for it is the same material used for the C_f calibration. Fig. 15 shows a very good accuracy for both the E_{IT} and H_{IT}, and hypothesis test as per Section 2.5 cannot reject the null hypothesis for the uncertainty bars overlap with the calibrated reference. The mechanical characterisation presents an average relative expanded uncertainty of 5% and 2.5% for E_{IT} and H_{IT}, respectively.

Similar results are obtained and shown in Fig. 16 for the Brass. In this case, a slightly higher relative expanded uncertainty is obtained, i.e. 7% and 5%, respectively for E_{IT} and H_{IT}, mostly due to the larger experimental data dispersion, which affects the reproducibility.

The characterisation of the stainless steels provides insights on the method performance and advantages. As Figs. 17 and 18 show, respectively for SSs and SSh, a constant bias can be appreciated with respect to the considered reference value obtained by nano- and micro-IIT. This result is consistent with the significant amount of pile-up that affects these materials at the calibration scales, as shown in Section 3.1. Consequently, these results show that, at the macro scale, if the frame compliance is correctly calibrated, i.e. catering for nonlinearities, accurate measurements of mechanical properties can be obtained, which could be potentially used as a reference for correcting nanoindentation results when affected by significant pile-up. The relative expanded uncertainty of the mechanical characterisation for the SS is 5.5% for E_{IT} and 2% for H_{IT}.

Last, the characterisation results are obtained for validation purposes to estimate the frame compliance trend on the materials. A regression model is applied independently per each material, and, as Fig. 19 shows, the data from different material superimposes. This validates the

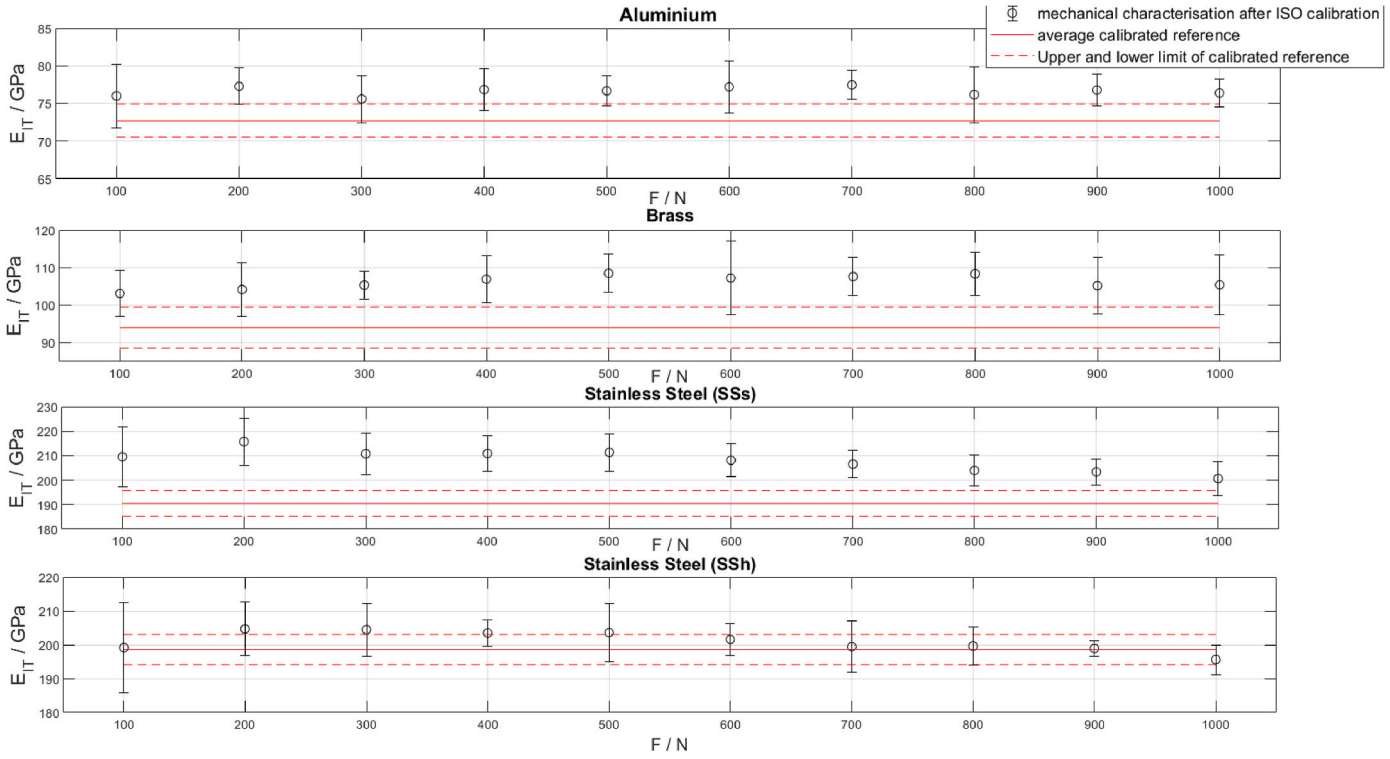

Fig. 10. Mechanical characterisation results of indentation modulus after calibrating the frame compliance with ISO method on SSh. Notice a significative trend of the results inconsistent with the definition of E_{IT} and a bias with respect to the calibrated value.

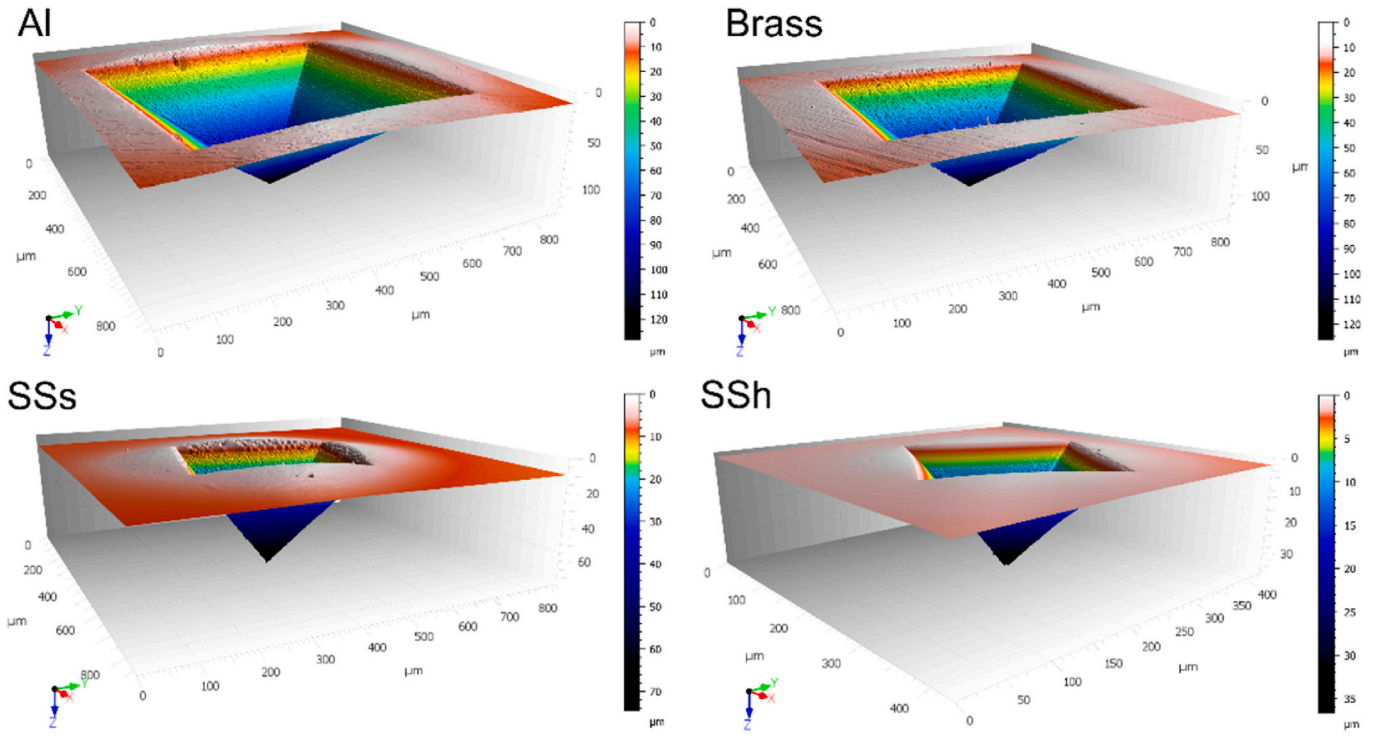

Fig. 11. Surface topographical measurement of an indentation per each considered sample performed at 400 N. No relevant pile-up can be appreciated. See supplementary material for further insights on the indentation topography.

obtained frame compliance estimations from the four materials, for they are not statistically different, with a risk of error of 5%.

4. Conclusions

This work proposed and successfully applied a simple and cost-effective method to calibrate the frame compliance, catering for its

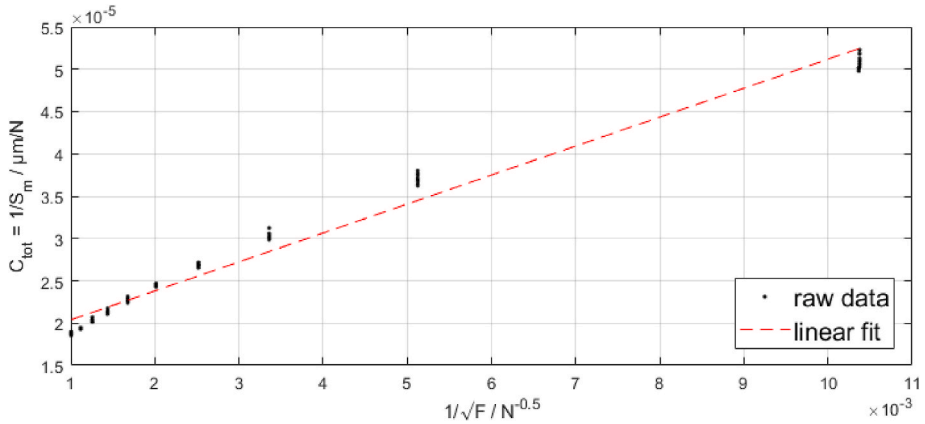

Fig. 12. Total compliance as a function of the inverse of the square root of the force. The assumption of constant frame compliance entails a linear trend of the total compliance. Notice the clear nonlinearity that disproof the hypothesis.

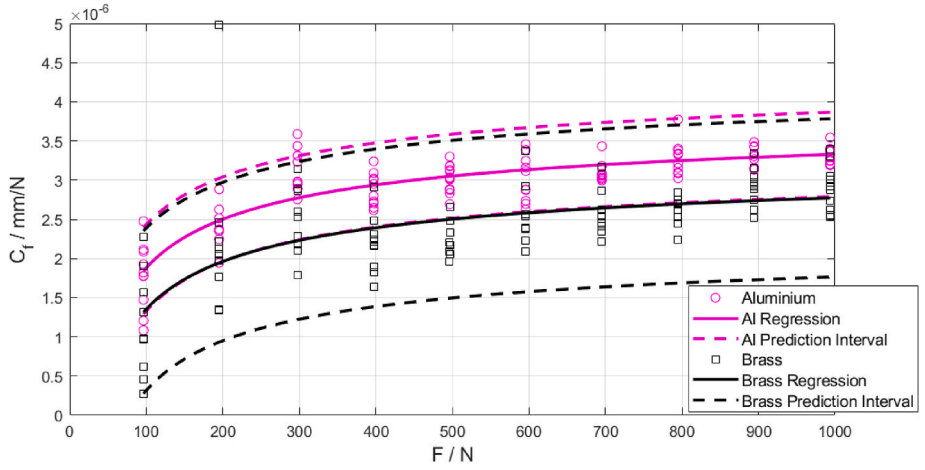

Fig. 13. Nonlinear frame compliance calibration fitting results using as calibrated reference material Aluminium (magenta) and Brass (black). Dashed lines represent prediction intervals at a 95% confidence level. Notice the superimposition of the prediction intervals, which statistically cannot disprove the compatibility of the two estimates.

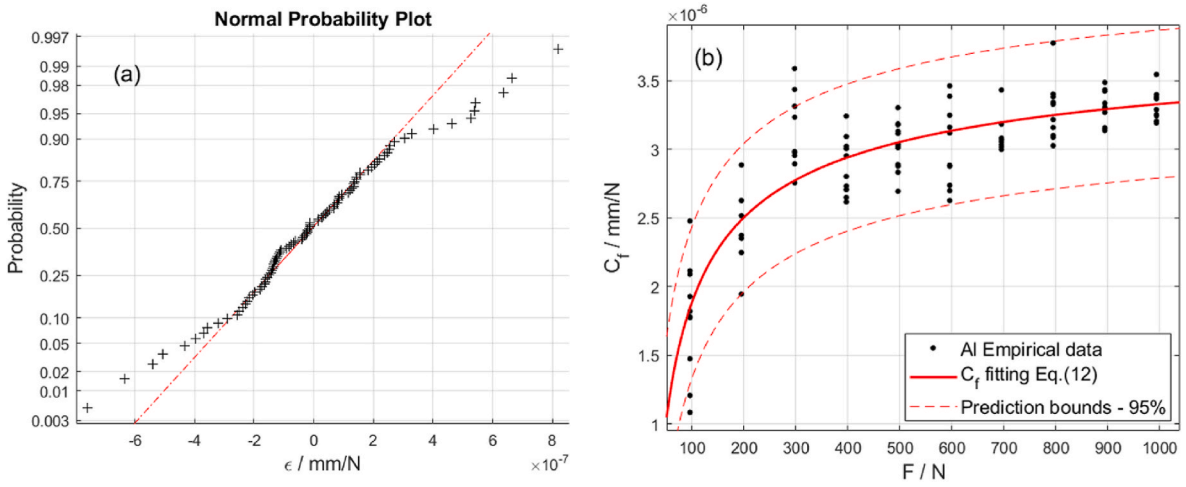

Fig. 14. Nonlinear frame compliance calibration fitting results. (a) NPP of the residuals, tails suggest a slight tendency to overfitting. (b) linear regression results with prediction interval.

nonlinearity. In particular, this work demonstrated that.

- the constant frame compliance assumption introduces significant errors in the mechanical characterization when different materials are tested;

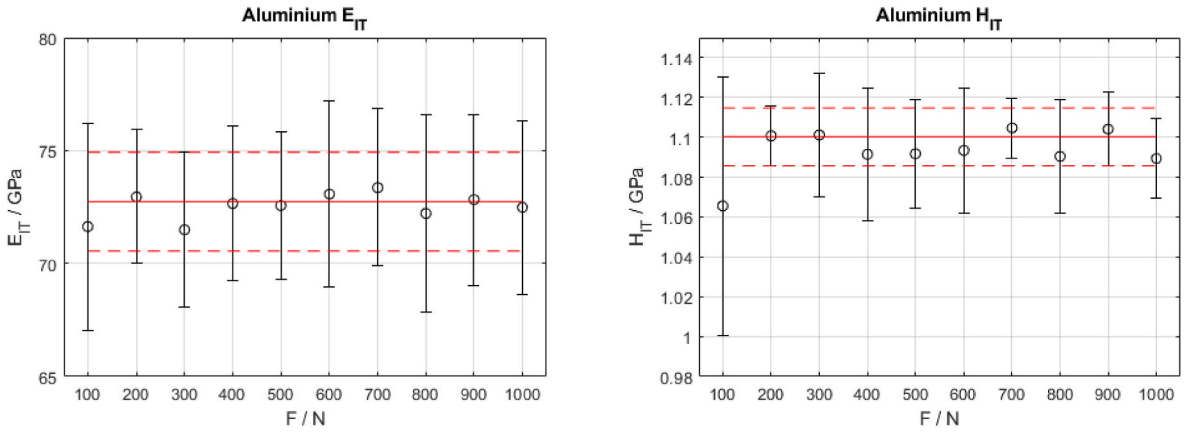

Fig. 15. Aluminium characterisation considering nonlinear frame compliance calibration. Black: characterisation results, red: calibrated reference (Section 3.1). Notice good accuracy in the validation of the calibration. Poor results at 100 N are associated with worse performances of the machine at the lower end of the working range. (For interpretation of the references to colour in this figure legend, the reader is referred to the Web version of this article.)

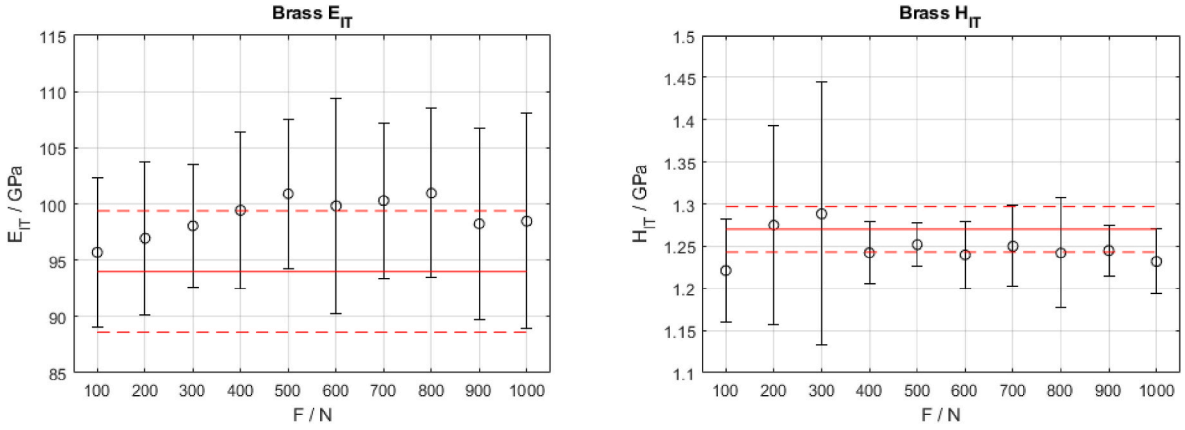

Fig. 16. Brass characterisation considering nonlinear frame compliance calibration. Black: characterisation results, red: calibrated reference (Section 3.1). Notice good accuracy in the agreement with the calibrated reference, even if a slight statistically non-significant trend can be seen in the E_{IT}. (For interpretation of the references to colour in this figure legend, the reader is referred to the Web version of this article.)

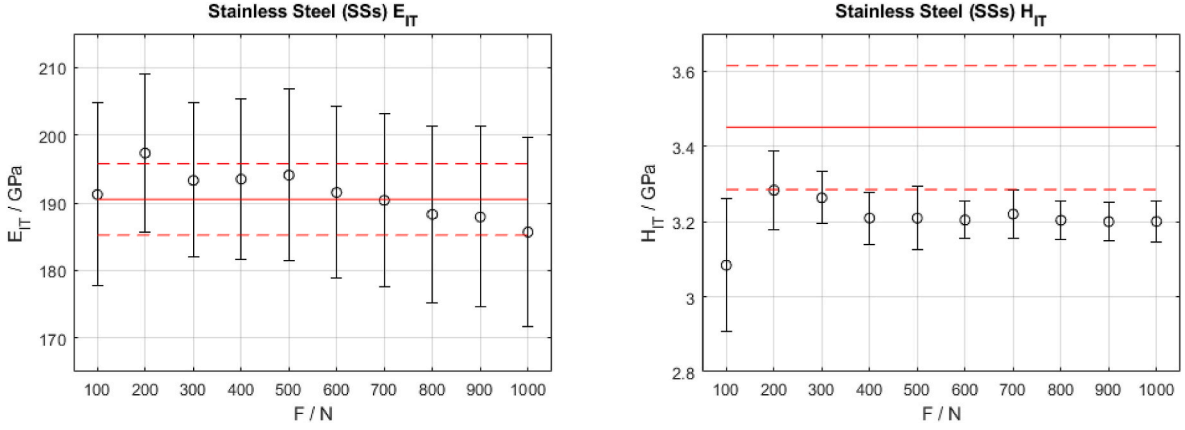

Fig. 17. Softer stainless steel (SSs) characterisation considering nonlinear frame compliance calibration. Black: characterisation results, red: calibrated reference (Section 3.1). Notice a slight statistically non-significant trend in the E_{IT} and a constant systematic difference with respect to the reference H_{IT}. (For interpretation of the references to colour in this figure legend, the reader is referred to the Web version of this article.)

- the claim that such errors might be ascribed to edge effect plasticity in the macro-range is disproved by a qualitative and quantitative analysis based on surface topography measurements;
- the proposed non-linear frame compliance calibration methodology provides compatible results independently of the reference material used;
- nano- and micro-IIT proved effective in calibrating materials that do not suffer from edge effects;

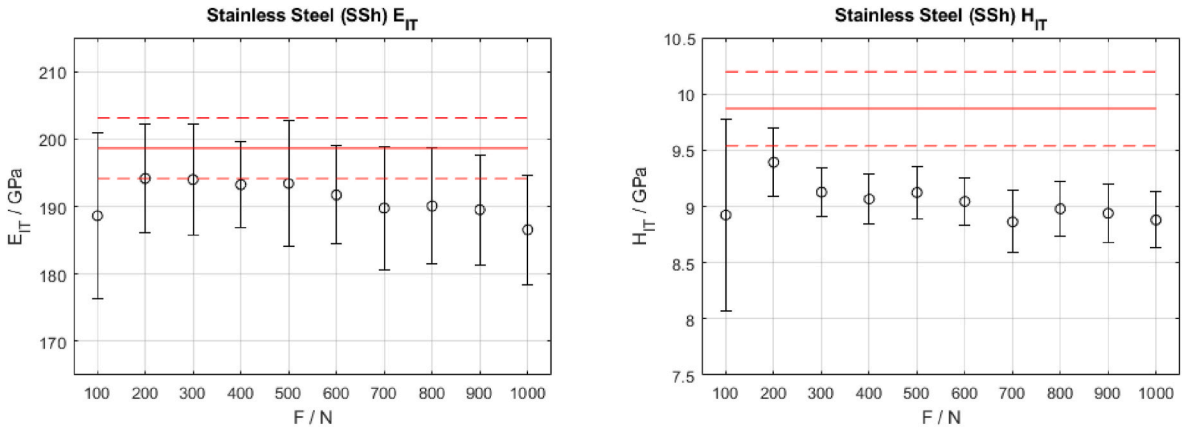

Fig. 18. Harder stainless steel (SSh) characterisation considering nonlinear frame compliance calibration. Black: characterisation results, red: calibrated reference (Section 3.1). Notice a slight statistically non-significant trend in the E_{IT} and a constant systematic difference with respect to the reference H_{IT}. (For interpretation of the references to colour in this figure legend, the reader is referred to the Web version of this article.)

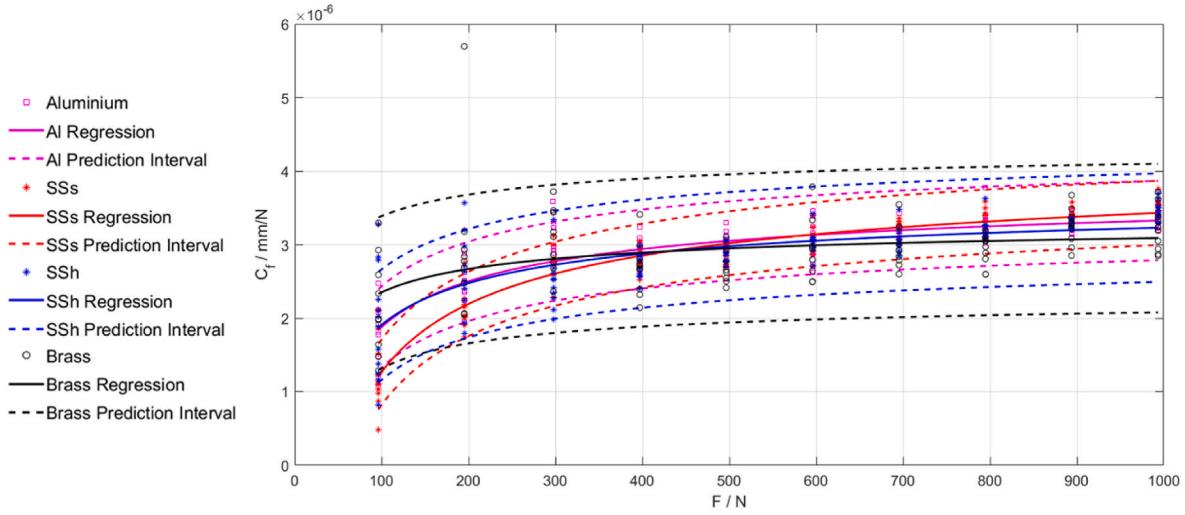

Fig. 19. Frame compliance evaluated as per Eq. (8) as a function of the maximum characterisation force for the four materials. Notice the good superimposition both in terms of average fitted trend and the superimposition of the prediction interval which statistically cannot reject the hypothesis of the material independence of the calibrated frame compliance.

- using such calibrated reference materials to calibrate the macro range indentation platform, accurate and precise characterization of mechanical properties can be obtained.

Future works will rely on the obtained results to exploit macro-instrumented indentation test to estimate correction approaches for characterization at force scale affected by edge-effect, e.g. micro range.

Declaration of competing interest

The authors declare that they have no known competing financial interests or personal relationships that could have appeared to influence the work reported in this paper.

Acknowledgements

This work has been partially supported by “Ministero dell’Istruzione, dell’Università e della Ricerca”. Award “TESUN-83486178370409 finanziamento dipartimenti di eccellenza CAP. 1694 TIT. 232 ART. 6”.

Appendix A. Supplementary data

Supplementary data to this article can be found online at https://doi.org/10.1016/j.precisioneng.2023.02.005.

References

[1] ISO 14577-1. Metallic materials — instrumented indentation test for hardness and material parameters - Part 1: test method. Genève: ISO; 2015.
[2] Galetto M, Genta G, Maculotti G. Single-step calibration method for nano indentation testing machines. CIRP Ann 2020;69:429–32. https://doi.org/10.1016/j.cirp.2020.03.015.
[3] Engqvist H, Wiklund U. Mapping of mechanical properties of WC–Co using nanoindentation. Tribol Lett 2000;8:147–52. https://doi.org/10.1023/A:1019143419984.
[4] Maculotti G, Senin N, Oyelola O, Galetto M, Clare A, Leach R. Multi-sensor data fusion for the characterisation of laser cladded cermet coatings. In: Eur Soc Precis Eng Nanotechnology, Conf Proc - 19th Int Conf Exhib EUSPEN; 2019. p. 260–3. 2019.
[5] Hou X, Jennett NM, Parlinska-Wojtan M. Exploiting interactions between structure size and indentation size effects to determine the characteristic dimension of nano-structured materials by indentation. J Phys D Appl Phys 2013;46. https://doi.org/10.1088/0022-3727/46/26/265301.
[6] Lee H, Mall S, He P, Shi D, Narasimhadevara S, Yun YH, Shanov V, Schulz MJ. Characterization of carbon nanotube/nanofiber-reinforced polymer composites using an instrumented indentation technique. Compos B Eng 2007;38:58–65. https://doi.org/10.1016/j.compositesb.2006.04.002.

[7] Cagliero R, Maizza G, Barbato G. Unconventional mechanical testing for process set up and product qualification in additive manufacturing. Polaris Innov J 2016;25:28–32.
[8] Maculotti G, Bonù S, Bonù L, Cagliero R, Genta G, Marchiandi G, Galetto M. Analysis of residual plastic deformation of blanked sheets out of automotive aluminium alloys through hardness map. IOP Conf Ser Mater Sci Eng 2021;1193:0120102. https://doi.org/10.1088/1757-899X/1193/1/012102.
[9] Maculotti G, Genta G, Lorusso M, Galetto M. Assessment of heat treatment effect on AlSi10Mg by selective laser melting through indentation testing. Key Eng Mater 2019;813:171–7. https://doi.org/10.4028/www.scientific.net/KEM.813.171.
[10] Lee J, Lee K, Lee S, Kwon OM, Kang WK, Lim J Il, Lee HK, Kim SM, Kwon D. Application of macro-instrumented indentation test for superficial residual stress and mechanical properties measurement for HY steel welded t-joints. Materials 2021;14(8):2061. https://doi.org/10.3390/ma14082061.
[11] Wehrstedt A, Ullner C. Standardization of the instrumented indentation test: historical development and comments. Mater Test 2004;46:106–12. https://doi.org/10.3139/120.100567.
[12] Galetto M, Genta G, Maculotti G, Verna E. Defect probability estimation for hardness-optimised parts by selective laser melting. Int J Precis Eng Manuf 2020;21:1739–53. https://doi.org/10.1007/s12541-020-00381-1.
[13] Schiavi A, Origlia C, Germak A, Barbato G, Maizza G, Genta G, Cagliero R, Coppola G. Indentation modulus at the macro-scale level measured by Brinell and Vickers indenters by using the primary hardness standard machine at INRiM. Acta IMEKO 2019;8:3–12. https://doi.org/10.21014/acta_imeko.v8i1.650.
[14] Schiavi A, Origlia C, Germak A, Prato A, Genta G. Indentation modulus, indentation work and creep of metals and alloys at the macro-scale level: experimental insights into the use of a primary vickers hardness standard machine. Materials 2021;14(11):2912. https://doi.org/10.3390/ma14112912.
[15] Maculotti G, Genta G, Carbonatto A, Galetto M. Uncertainty-based comparison of the effect of the area shape function on material characterisation in nanoindentation testing. Eur Soc Precis Eng Nanotechnology, Conf Proc – 22nd Int Conf Exhib EUSPEN 2022:361–4.
[16] Oliver WC, Pharr GM. An improved technique for determining hardness and elastic modulus using load and displacement sensing indentation experiments. J Mater Reseach 1992;7:1564–83.
[17] Genta G, Maculotti G, Barbato G, Levi R, Galetto M. Effect of contact stiffness and machine calibration in nano-indentation testing. Procedia CIRP 2018;78:208–12. https://doi.org/10.1016/j.procir.2018.08.313.
[18] Cagliero R, Barbato G, Maizza G, Genta G. Measurement of elastic modulus by instrumented indentation in the macro-range: uncertainty evaluation. Int J Mech Sci 2015;101–102:161–9. https://doi.org/10.1016/j.ijmecsci.2015.07.030.
[19] Maculotti G, Genta G, Lorusso M, Pavese M, Ugues D, Galetto M. Instrumented indentation test: contact stiffness evaluation in the nano-range. Nanomanufacturing Metrol 2019;2(1):16–25. https://doi.org/10.1007/s41871-018-0030-y.
[20] ISO 14577-2. Metallic materials-Instrumented indentation test for hardness and materials parameters-Part 2: verification and calibration of testing machines. Genève: ISO; 2015.
[21] Barbato G, Genta G, Cagliero R, Galetto M, Klopfstein MJ, Lucca DA, Levi R. Uncertainty evaluation of indentation modulus in the nano-range: contact stiffness contribution. CIRP Ann - Manuf Technol 2017;66:495–8. https://doi.org/10.1016/j.cirp.2017.04.060.
[22] Ullner C, Reimann E, Kohlhoff H, Subaric-Leitis A. Effect and measurement of the machine compliance in the macro range of instrumented indentation test. Meas J Int Meas Confed 2010;43:216–22. https://doi.org/10.1016/j.measurement.2009.09.009.
[23] Ullner C. Critical points in ISO 14577 part 2 and 3 considering the uncertainty in measurement. Proc of HARDMEKO 2004;1–5.
[24] Chudoba T, Schwenk D, Reinstädt P, Griepentrog M. High-precision calibration of indenter area function and instrument compliance. JOM (J Occup Med) 2022;74:2179–94. https://doi.org/10.1007/s11837-022-05291-3.
[25] Galetto M, Maculotti G, Genta G, Barbato G, Levi R. Instrumented indentation test in the nano-range: performances comparison of testing machines calibration methods. Nanomanufacturing Metrol 2019;2:91–9. https://doi.org/10.1007/s41871-019-00035-5.
[26] Maculotti G, Genta G, Galetto M. Criticalities of iterative calibration procedures for indentation testing machines in the nano-range. Proc. 20th Int. Conf. Exhib. EUSPEN, Genève: Euspen 2020:2–5.
[27] Moharrami N, Bull SJ. A comparison of nanoindentation pile-up in bulk materials and thin films. Thin Solid Films 2014;572:189–99. https://doi.org/10.1016/j.tsf.2014.06.060.
[28] Taljat B, Zacharia T, Pharr GM. Pile-up behavior of spherical indentations in engineering materials. MRS Proc 1998;522:33. https://doi.org/10.1557/PROC-522-33.
[29] Cheng YT, Cheng CM. Effects of 'sinking in' and 'piling up' on estimating the contact area under load in indentation. Phil Mag Lett 1998;78:115–20. https://doi.org/10.1080/095008398178093.
[30] N'jock MY, Chicot D, Ndjaka JM, Lesage J, Decoopman X, Roudet F, et al. A criterion to identify sinking-in and piling-up in indentation of materials. Int J Mech Sci 2015;90:145–50. https://doi.org/10.1016/j.ijmecsci.2014.11.008.
[31] Fay TH, Joubert SV. Energy and the nonsymmetric nonlinear spring. Int J Math Educ Sci Technol 1999;30:889–902. https://doi.org/10.1080/002073999287554.
[32] Champion R, Champion WL. Departure from linear mechanical behaviour of a helical spring. Math Comput Model 2011;53:915–26. https://doi.org/10.1016/j.mcm.2010.10.028.
[33] ISO 376. BSI Standards Publication Metallic materials — calibration of force-proving instruments used for the verification of uniaxial testing machines. Genève: ISO; 2011.
[34] Hellier CJ. Handbook of nondestructive evaluation. second ed. second ed. New York: McGraw-Hill Education; 2013.
[35] Nix WD, Gao H. Indentation size effects in crystalline materials: a law for strain gradient plasticity. J Mech Phys Solid 1998;46:411–25. https://doi.org/10.1016/S0022-5096(97)00086-0.
[36] Hou XD, Bushby AJ, Jennett NM. Study of the interaction between the indentation size effect and Hall-Petch effect with spherical indenters on annealed polycrystalline copper. J Phys D Appl Phys 2008;41. https://doi.org/10.1088/0022-3727/41/7/074006.
[37] de Groot P. Coherence scanning interferometry. In: Leach RK, editor. Opt. Meas. Surf. Topogr. Berlin: Springer-Verlag; 2011. p. 187–208.
[38] Chudoba T, Richter F. Investigation of creep behaviour under load during indentation experiments and its influence on hardness and modulus results. Surf Coating Technol 2001;148:191–8. https://doi.org/10.1016/S0257-8972(01)01340-8.
[39] JCGM100. Evaluation of measurement data — Guide to the expression of uncertainty in measurement (GUM). JCGM 2008:Sèvres, France. 2008. https://doi.org/10.1373/clinchem.2003.030528.